New Global Mean Dynamic Topography CNES-CLS-22 Combining Drifters, Hydrological Profiles and High Frequency Radar Data

Solène Jousset[1], Sandrine Mulet[1], Eric Greiner[1], John Wilkin[2], Lien Vidar[3], Gérald Dibarboure[2], and Nicolas Picot[4]

[1]CLS, Ramonville Saint Agne, 31250, France
[2]Affiliation not available
[3]Institute of Marine Research, Bergen, Norway
[4]CNES, Ramonville Saint Agne, 31520, France

December 3, 2023

Abstract. The mean dynamic topography (MDT) is a key reference surface for altimetry. It is needed for the calculation of the ocean absolute dynamic topography, and under the geostrophic approximation, the estimation of surface currents. CNES-CLS mean dynamic topography (MDT) solutions are calculated by merging information from altimeter data, GRACE, and GOCE gravity field and oceanographic in situ measurements (drifting buoy velocities, High Frequency radar velocities, hydrological profiles). The objective of this paper is to present the newly updated CNES-CLS22 MDT. The main improvement of this new CNES-CLS22 MDT over the previous CNES-CLS18 MDT is in the Arctic, with better coverage, no artifacts and a more realistic solution. This is due to the use of a new first guess estimated with the CNES-CLS22 MSS and the GOCO06s geoid to which optimal filtering has been applied, as well as Lagrangian filtering at the coast to reduce the intensity of normal currents at the coast. Improvements also include updating the drifting buoy and T/S profile databases, as well as processing to obtain synthetic mean geostrophic velocities and synthetic mean heights. In addition, a new data type, HF radar data, was processed to extract physical content consistent with MDT in the Mid Atlantic Bight region. The study of this region in particular has shown the improvements of the CNES-CLS22 MDT, but that there is still work to be done to obtain a more physical solution over the continental shelf. The CNES-CLS22 MDT has been evaluated against independent height and velocity data in comparison with the previous version, the CNES-CLS18. The new solution presents slightly better results, although not identical in all regions of the globe.

1 Introduction

Since the early days of altimetry, estimating absolute dynamic topography (ADT) accurately has been an issue (Rio 2010). The absence of an accurate geoid at spatial scales corresponding to the spatial resolution of altimetry data along tracks, i.e. 7km at 1Hz and 300m at 20Hz, does allow to reconstruct absolute dynamic topography accurately. So most scientific studies of the ocean have used the temporally variable part of sea level relative to the mean over a reference period: the sea level anomaly (SLA). And this has improved our knowledge of the dynamics of mesoscale structures. However, many scientific and operational activities require accurate absolute sea level. For the study of eddy-mean interactions, a positive sea level anomaly can be due to different processes such as anticyclonic eddies, the strengthening of a quasi-permanent anticyclonic eddy, the weakening of a cyclonic eddy, or the displacement of a current or eddy (Rio et al. 2007; Pegliasco et al. 2020). Pegliasco et al. (2020) shows that it is more appropriate to use absolute dynamic topography rather than SLA to track eddies. For the correct assimilation of altimetry data into models, Hamon et al.

(2019) have highlighted the need for an accurate MDT as well as its associated error. Finally, absolute dynamic topography provides access to geostrophic currents, useful data for monitoring ocean currents, and different application as maritime security, ocean pollution.

Furthermore, with the arrival of new swath observations from the SWOT (Surface Water and Ocean Topography) satellite launched in December 2022 (Fu et al. 2012), which provides sea level observations over swaths 120 km wide with a resolution of 2 km, an accurate MDT at a spatially finer resolution and defined close to the coast is needed.

To access the absolute dynamic topography, it is necessary to estimate an accurate Mean Dynamic Topography (MDT ; ADT = MDT + SLA). Since the launch of the ESA GOCE satellite (Gravity and Ocean Circulation Experiment; Pail et al. 2011), the Earth's geoid has been measured with centimetric accuracy at a spatial resolution of 100km. In addition, the accumulation of altimetry data, improved processing and, in recent years, the special processing applied to leads (fractures in ice) have led to an improvement in the Mean Sea Surface (MSS) and its estimation over ice-covered areas such as the Artic Ocean (Schaeffer et al. 2023). The "geodetic" approach (Bingham et al. 2008), which consists of estimating the MDT by subtracting the geoid from the MSS, then applying a reliable filter, provides accurate solutions for spatial scales greater than 100km. To estimate spatial scales shorter than 100km, it is necessary to add information to these scales. A first method is to use altimetry data to add finer scales to the geoid. These geoids are called combined geoids, Eigen6c4 (Förste et al. 2014) and XGM2019e (Zingerle et al. 2020) are examples. From these combined geoids, it is possible to estimate a geodetic MDT such as MDT DTU22 (Knudsen et al. 2022). Another approach is to use a large-scale satellite-only geodetic MDT and add the small scales from in-situ ocean data (temperature and salinity profiles, velocities estimated from drifting buoys or High Frequency radars). These in situ data need to be processed to extract only the physical content corresponding to the MDT. This approach is used to estimate the various CNES-CLS MDTs (Rio and Hernandez 2004; Rio et al. 2011; Rio et al. 2014; Mulet et al. 2021) and in this study.

This paper presents the new CNES-CLS22 Mean Dynamic Topography (MDT) solution. Improvement has been made possible by the recent availability of updated time series of drifter and in situ temperature and salinity profiles data, improved MSS and geoid model. The method is reminded in section 2, while data used in the computation and validation are presented in section 3. The new CNES-CLS22 MDT is described and validated in section 4. Conclusions and discussion are provided in section 5.

2 Method

The method used to estimate the new CNES-CLS2022 MDT follows the same approach than the one detailed in Rio and Hernandez (2004), Rio et al. (2007, 2011 and 2014a), and Mulet et al. (2021). It is a three-step approach reminded and summarized below:

The first step is to compute a first guess MDT from the filtered difference between the MSS and the geoid model: a geodetic MDT. The effective resolution of this resulting field depends on the noise level of the raw differences between the MSS and the geoid height; it is around 125km (Bruinsma et al. 2014).

The second step is to compute synthetic estimates of the MDT and associated mean geostrophic velocities from in-situ data. The drifter data and High Frequency (HF) radar data are processed to keep only the geostrophic component. For the dynamic heights estimated from the T/S profiles, they are processed to add the missing components: the barotropic component and the deep baroclinic component. Temporal variability is removed from the dynamic heights and velocities, by subtracting the altimeter sea level anomalies and the associated geostrophic velocity anomalies respectively. Since the altimeter sea level anomalies referenced to the 1993-2012 reference period, the processed in-situ dynamic heights and velocities are then also referenced to the 1993-2012 period, and this allows the use of in-situ observations over a longer period than the reference period (Rio and Hernandez 2004). The processed dynamic heights are averaged by 1/4° boxes to obtain the synthetic mean heights and the processed velocities are averaged by 1/8° boxes to obtain the synthetic mean velocities. Velocities from HF radar are averaged per cell (6X6km resolution). Note that this version of the MDT uses only Mid Atlantic Bight HF radar data.

Finally, the third step consists in improving the large-scale MDT (from step 1) from the synthetic data (from step 2) through a multivariate objective analysis whose formulation was first introduced in oceanography by Bretherton et al. (1976). This analysis takes as input the a-priori knowledge of the MDT variance and zonal and meridional correlation scales.

2.1 Computation of first guess and comparison with previous first guess

The raw difference between the CNES-CL22 MSS and GOCO06s geoid height is filtered using the optimal filter fully described in Rio et al. (2011). For the MDT CNES-CLS22 computation, this step has been improved with the application of additional Lagrangian filter along the coast to avoid streamline going into land.

The geostrophic velocities associated with the first guess calculated from the raw differences between the CNES-CL22 MSS and GOCO06s geoid height optimaly filtered are compared with the drifter velocities (section 3); the drifter velocities have been processed to obtain a physical content comparable with the geostrophic velocities. Similarly, the geostrophic velocities associated with the first guess of the CNES-CLS18 MDT have been compared with the drifter velocities. Figure 1 shows the improvement (blue color) or degradation (red color) of the RMS of the differences with the drifter velocities of the CNES-CLS22 first guess compared with the CNES-CLS18 first guess, in current amplitude (a) and current direction (b). Figure 1 (a) shows that current amplitude is strongly enhanced near the coast, almost everywhere. In the open ocean, the differences between the two first guesses in comparison to drifters are minimal, except south of 45°S, particularly in the Indian Ocean, where there are degradation boxes for first guess 2022. For this comparison, Lagrangian filtering at the coast has not yet been applied. This improvement at the coast in the amplitude of the geostrophic currents associated with the first guess compared with the drifters is linked to the use of the new CNES-CLS22 MSS and the new GOCO06s geoid. As for the current direction shown in Figure 1 (b), there is no clear improvement or deterioration in the new first guess compared with the old one.

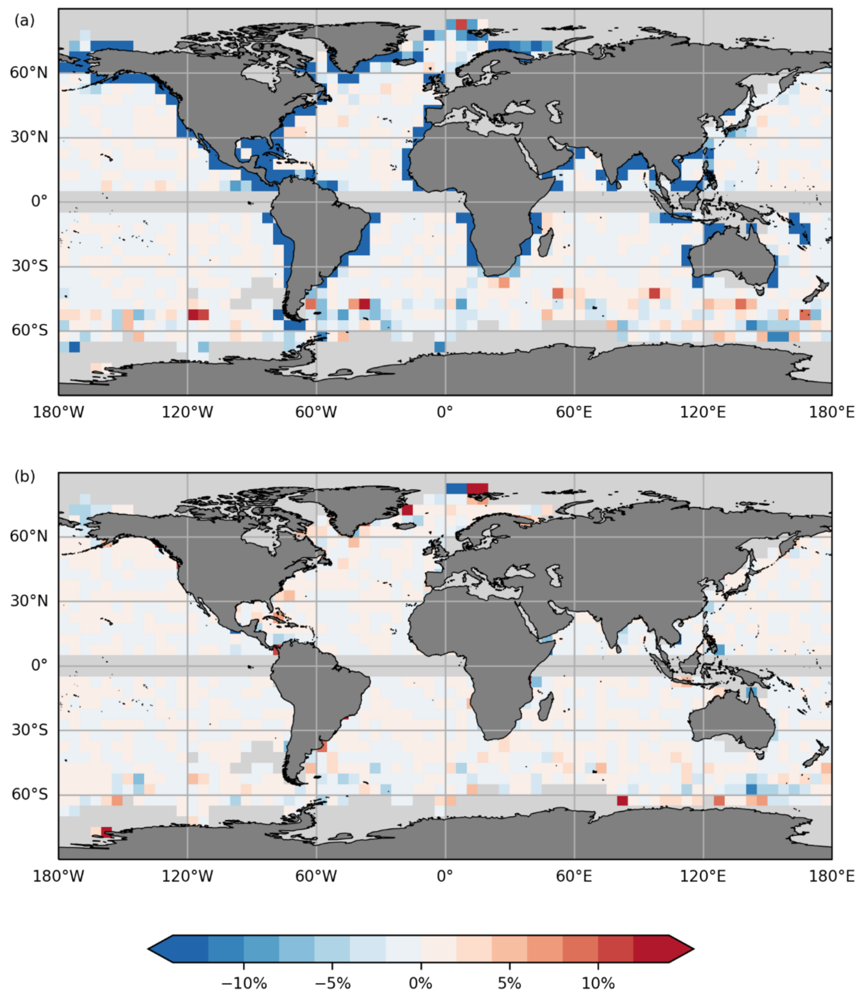

Figure 1: Comparison of the RMS of the differences (a) in current modulus and (b) in direction, of the independent drifting buoy velocities and the altimeter geostrophic velocities obtained using MDT solutions first guess of the CNES-CLS22 (unfiltered at the coast with the Lagrangian filter) and the first guess of the CNES-CLS18, in percent :

$\%\mathrm{RMSD} = \frac{\mathrm{RMS}(\mathbf{U}_{\mathrm{MDT}_{\mathbf{FG22}}}) - \mathrm{RMS}(\mathbf{U}_{\mathrm{MDT}_{\mathbf{FG18}}} - \mathbf{U_d})}{\mathrm{RMS}(\mathbf{U}_{\mathrm{MDT}_{\mathbf{FG18}}} - \mathbf{U_d})}$. These statistics are calculated in boxes of 5* by 5*. Only boxes with more than 100 measurement points and more than 10 different drifters are shown. The bluish colors denote improvement while reddish colors stand for degradation.

2.2 Computation of the synthetic mean heights

The aim of estimating synthetic mean heights is to use temperature and salinity profiles to calculate a mean height whose physical content is the same as the MDT. Temperature and salinity profiles are used to calculate density variations in the water column and to estimate a dynamic height (between the profile's reference depth and the surface) representing the baroclinic component of the dynamic circulation. Here we use reference depths of 200, 400, 900, 1200 and 1900m, with each dynamic height calculated according to one of these reference depths, the deepest accessible according to the maximum depth of the T/S profile. The dynamic heights thus estimated do not have the same physical content as the Altimeter Sea Level Anomalies

(SLA), as the SLA is also influenced by baroclinic processes between the reference depth and the bottom, as well as by barotropic processes not measured by change in temperature and salinity (Rio et al. 2014b). To obtain average heights over the reference period, we need to remove the temporal variability (of the SLA) from the instantaneous dynamic heights; we therefore need to remove the temporal variability by subtracting the part of the SLA corresponding to the baroclinic process from the surface to the reference depth. Then add the missing components: the barotropic signal and the baroclinic signal from the reference depth of the profile to the bottom. The method for these two steps is the same as the one fully described in Rio et al. (2011) and also used in Rio et al. (2014a) and in Mulet et al. (2021).

In particular, the missing quantity, the average contribution of deep baroclinic and barotropic processes, is estimated as the difference between the climatology of dynamic heights relative to the given reference depth, the same as the T/S profile and the first estimate of the CNES-CLS MDT22. For each reference depth considered in this study (200, 400, 900, 1200 and 1900m), a climatology is calculated from the same CORA database (section 3) to remain consistent, this time using the maximum number of profiles possible, i.e. for the reference depth 200m, using all profiles deeper than 200m. These climatologies are then filtered at the same spatial scale as the first guess, i.e. 125km.

The optimal analysis to estimate the CNES-CLS22 MDT is performed on the anomalies with respect to the first guess, so we remove the first guess from the synthetic fields before the optimal analysis and then add this first guess to the result to obtain the final MDT. In this remove-restore framework, the estimation of mean synthetic heights is equivalent to considering only the small scales of synthetic dynamic heights relative to reference depth. Figure 2 shows these fine scales of synthetic mean heights (all reference depths averaged by 1/8° by 1/8° boxes). The signal is intense in the large western boundary currents and in the Antarctic Circumpolar Current (ACC), with anomalies of over +/-10 cm. These mean synthetic heights will tend to accelerate these large currents.

Finally, the synthetic mean heights are averaged in 1/8* boxes. The associated errors are computed as described in Rio et al. (2011). These errors are high in areas of high oceanic variability: western boundary currents, the ACC; and near the poles, where there are few data or less confidence in processing. Overall, the error is less than 2cm in the rest of the ocean. As in the Rio et al. (2014b) study, the error associated with these mean synthetic heights does not take into account the first-guess error and is therefore certainly underestimated.

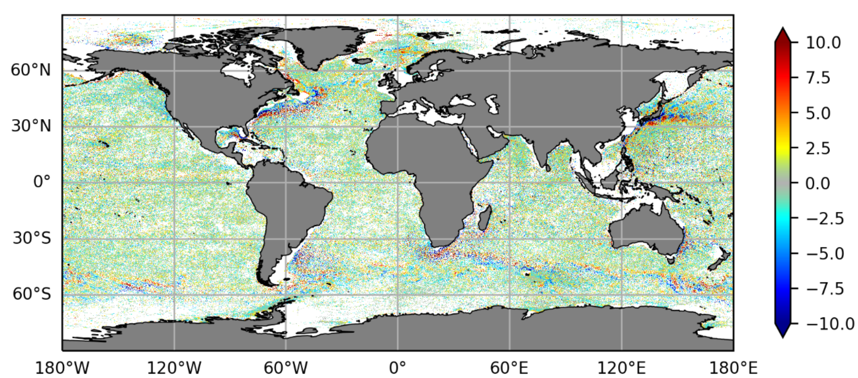

Figure 2: Fine scales of synthetic mean heights, all reference depths averaged by 1/8° by 1/8° boxes in cm, equivalent to mean synthetic heights minus first guess (input to optimal analysis).

2.3 Computation of the synthetic mean velocities

The objective of this estimation is to process the velocities estimated from drifters (section 3) and surface Argo float drifts to obtain the physical content of the geostrophic currents associated with the MDT. This is achieved by removing from the drifter velocities the ageostrophic components of the current, as well as the temporal variability of the geostrophic component of the velocities:

$$U_{\text{synth}} = U_{\text{drifter}} - U_{\text{Ekman}} - U_{\text{Stokes}} - U_{\text{inertial}} - U_{\text{tidal}} - U_{ageo-hf} - U_{\text{slippage}} - U'_{\text{alti}}$$

First, wind-driven currents (U_{Ekman}) is removed from the drifter velocity, as well as the wind slippage (U_{slippage}), which is the direct effect of wind on undrogued drifters. U_{Ekman} is taken from the Copernicus-Globcurrent product (MULTIOBS_GLO_PHY_REP_015_004, *https://data.marine.copernicus.eu/product/MULTIOBS_GLO_PHY_REP_015_004/description*) while wind slippage correction (U_{slippage}) is available in the CMEMS INSITU_GLO_PHY_UV_DISCRETE_MY_013_044 product (*https://data.marine.copernicus.eu/product/INSITU_GLO_PHY_UV_DISCRETE_MY_013_044/description*). These products are consistent as they use same upstreams for computation: ERA5 wind and wind stress (section 3), and Mixed Layer Depth as a proxy to the Ekman layer thickness (from CMEMS ARMOR3D: MULTIOBS_GLO_PHY_TSUV_3D_MYNRT_015_012, *https://data.marine.copernicus.eu/product/MULTIOBS_GLO_PHY_TSUV_3D_MYNRT_015_012/description*). Then the temporal variability of the geostrophic component of velocities (U'_{alti}) is removed. Next, the tide, inertial oscillations and residual ageostrophic signal (as U_{stokes}) are removed by high-frequency filtering. Finally, the mean synthetic velocities obtained are averaged in boxes 1/8° by 1/8°.

This method, the estimation of the wind-driven component of the current and slippage, and the filtering applied are fully described in Mulet et al. (2021, section 5) and build on previous work by Rio and Hernandez (2004), Rio et al. (2007, 2011 and 2014a).

For this new MDT, we are also using velocities data estimated from High Frequency radars located in the Mid Atlantic Bight area, on the East Coast of the USA, from Cape Hatteras to Cape Cod. In the same way as for drifter data, the aim is to process these velocities to obtain synthetic velocities with the physical content of geostrophic MDT velocities. We used the cleaned, detited, high-frequency signal-filtered and mean currents over the period 2006-2016, processed by Rutgers University (Roarty et al. 2020). Then the mean wind-driven currents over the same period (U_{Ekman} taken from the Copernicus-Globcurrent product MULTIOBS_GLO_PHY_REP_015_004) were removed and finally these mean currents were re-referenced to the 1993-2012 reference period.

Figure 3 shows these mean synthetic velocities estimated from (a) drifters (at 1/8° resolution) and (b) HF radar data, over the Mid Atlantic Bight area off New Jersey and Delaware (USA). The figure also shows the 100m and 2000m isobaths that mark the limit of the continental shelf. The average synthetic velocities estimated by drifters are much noisier, with more intense currents, than those estimated from HF radars. However, both maps show a recirculation current to the south-east at the 100m isobath. The drifters (Figure 3 a) show this current as narrow and intense (15 to 20 cm/s), whereas the HF radars (Figure 3 b) show a broad current of between 5 and 10 cm/s. Very close to the coast, velocities are generally low (below 5 cm/s), but currents can be perpendicular to the coast (e.g. Figure 3 b at 74.5°, 75° and 75.5°W). Between 74.9° and 75°W, the outflow of the Delaware River could explain these cross-shore currents.

These differences can be explained by the very different sampling of the two types of data:

- HF radar: at least 50% of data every hour over 10 years

- Drifters (1 or 2 drifters per box near the coast).

Moreover, it is likely that drifters tend to converge at the center of the current due to convergence and subduction, resulting in a sampling bias in favor of a narrow jet.

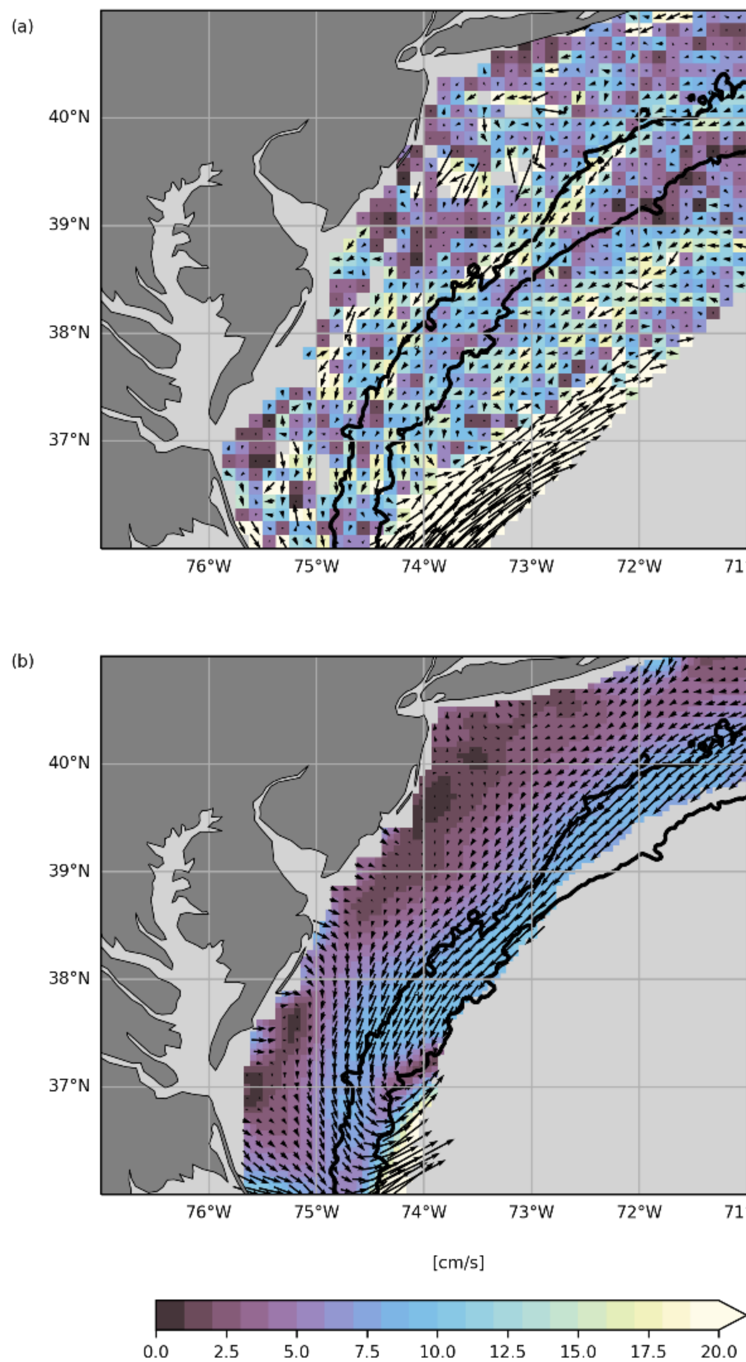

Figure 3: Synthetic mean velocities in the Mid Atlantic Bight region off New Jersey and Delaware, estimated (a) from drifting buoy (at 1/8°) and (b) from HF radar data. Black lines represent 100m and 2000m isobaths.

2.4 Multivariate objective analysis

The third step of this method is multivariate objective analysis as in Rio and Hernandez (2004), Rio et al. (2007, 2011 and 2014a) and in Mulet et al. (2021), which uses the synthetic mean geostrophic velocities and synthetic mean heights to improve the first guess, in particular to improve the fine scales, to obtain the CNES-CLS22 MDT. This optimal analysis requires the a priori MDT variance and the a priori zonal and meridional spatial correlation scales of the estimated field. The same statistical a priori as for Rio et al. (2014a) and Mulet et al. (2021) are used here. In the equatorial band, as the geostrophic approximation is no longer valid, only mean synthetic height observations are used for MDT estimation, and for current estimation, only mean synthetic velocities observations are used for inversion.

3 Data

The CNES-CLS22 MDT is calculated from a combination of altimeter and space gravity data, in situ measurements and model winds. The method allows us to estimate the mean over the 1993-2012 reference period, but is not limited to observations from this period. For each in situ observation, we remove the altimetric variability referenced to the 1993-2012, thus obtaining an estimate of the mean dynamic topography corresponding to the reference period. The following datasets are used:

– *MSS.* The CNES-CLS22 MSS derived for the 1993– 2012 reference time period by Schaeffer et al. (2023) is used.

– *Geoid model.* The satellite-only geoid model GOCO06s (Kvas et al. 2021) is used with the CNES-CLS22 MSS in the computation of the MDT first guess.

– *Altimeter sea level anomalies (SLAs).* The DUACS-2021 (Taburet et al. 2022) multimission gridded sea level and derived geostrophic velocity anomaly products distributed by the Sea Level Thematic Assembly Center (SL-TAC) from the CMEMS altimeter are used.

– *Dynamic heights.* These are calculated from temperature and salinity (T/S) profiles from CTD and ARGO from CMEMS CORA Release November 2022 (period 1993-2020, Szekely et al. 2023), processed by the In Situ Thematic Assembly Center (INS-TAC) of the Copernicus Marine Environment and Monitoring Service (CMEMS). In order to carry out a cross-validation of the new CNES-CLS22 MDT with the latest CNES-CLS18 MDT (Mulet et al. 2021), about 5% of the T/S profiles which will not be used for the calculation of the MDT, is kept. These 5% of the T/S profiles are randomly selected since 2017, in order to have a set of validation data that is independent of the new MDT but also of the CNES-CLS18 MDT.

– *In situ velocities.* Two types of in situ drifting buoy velocities are used, the 6-hourly SVP-type drifter distributed by the Surface Drifter Data Assembly Center (SD-DAC; Lumpkin and Johnson 2013) and the Argo floats surface velocities from the regularly updated YOMAHA07 dataset for the period 1997–2021 (Lebedev et al. 2007). SVP-type drifters consist of a spherical buoy with a drogue attached in order to minimize the direct wind slippage and follow the ocean currents at a nominal 15 m depth. When the drogue gets lost, the drifter is then advected by the surface currents and the direct action of the wind. In this study both the 15 m drogued and the surface undrogued drifter velocities over the 1993– 2021, period are considered for the MDT calculation. 10% of the AOML drifters dataset are randomly selected after 2017 and kept for validation of the results (independent data from CNES-CLS22 and CNES-CLS18). This new CNES-CLS22 MDT also uses velocity data estimated from HF radars located in the Mid Atlantic Bight area, East coast of the US from Cape Hatteras to Cape Cod. We used the cleaned, detited, high-frequency signal-filtered and mean currents over the period 2006-2016 (processed by Rutgers University, Roarty et al. 2020).

– *Wind data.* Wind stress data are needed for the calculation of the wind-driven velocities (Sect. 2.3) that is used to remove part of the ageostrophic component from drifter velocities. We use the 3-hourly, 80 km resolution wind stress fields from ERA5 (Hersbach et al. 2018) for the period 1993–2021.

4 Results

4.1 High-resolution CNES-CLS2022 MDT and associated currents

The CNES-CLS22 MDT obtained is shown on Figure 4 (a) and the amplitude of the associated geostrophic currents is displayed in Figure 4 (b). Compared with the first guess, the CNES-CLS22 MDT contains more small scales, gradients are tighter and currents are accelerated. Figure 5 also shows a zoom of this new CNES-CLS22 MDT (a) and the amplitude of the associated geostrophic currents (b) over the Artic zone, as well as a zoom of the CNES-CLS18 MDT (c) and the amplitude of the associated currents (d). Firstly, we note that the CNES-CLS22 MDT covers the Artic zone, which was not the case before. This is due to the improved coverage of the CNES-CLS22 MSS used to estimate the first guess of this new MDT. Artifacts present on the CNES-CLS18 MDT have disappeared from the new version, for example around 110-120°E. Moreover, Beaufort gyre is better resolved and Pan Arctic transport is visible. On the other hand, the Beaufort Gyre tends to "spread out" over the Canadian Archipelago, which is not physical. In this area of the Canadian Archipelago, the CNES-CLS22 MSS is slightly weaker (Schaeffer et al. 2023), which probably explains the poor physical representation of the CNES-CLS22 MDT. Furthermore, the reliability of MDT is lower in areas where observations are rare or absent, so results must be interpreted with caution in these areas; in the European Arctic, the Kara Sea is an example of such sparsely observed areas.

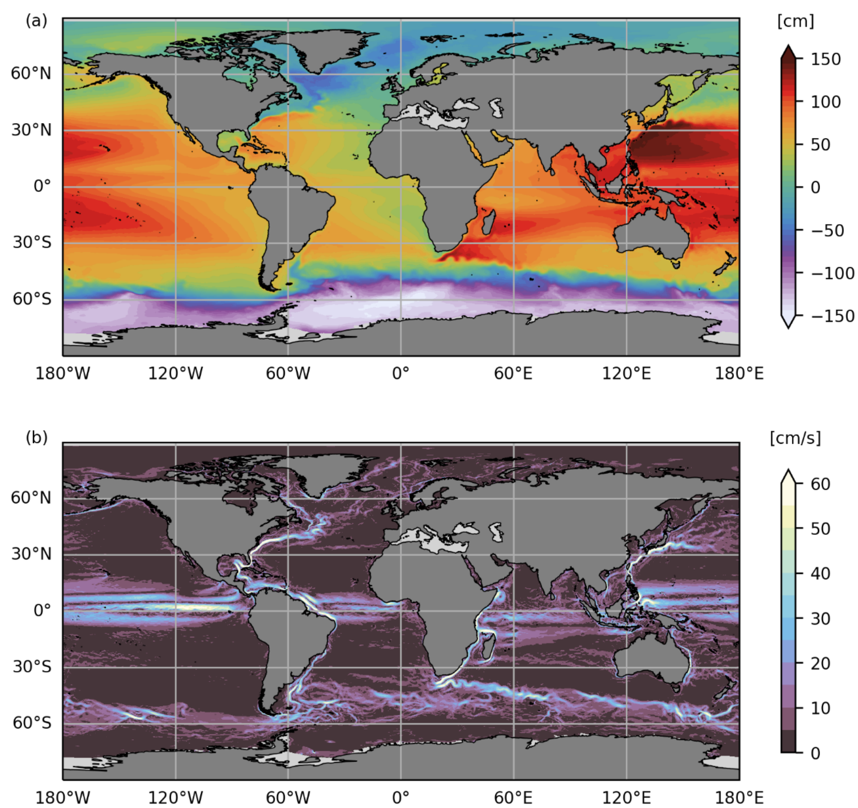

Figure 4: (a) The CNES-CLS22 MDT (cm) and (b) and the amplitude of the geostrophic currents associated with this MDT (cm/s).

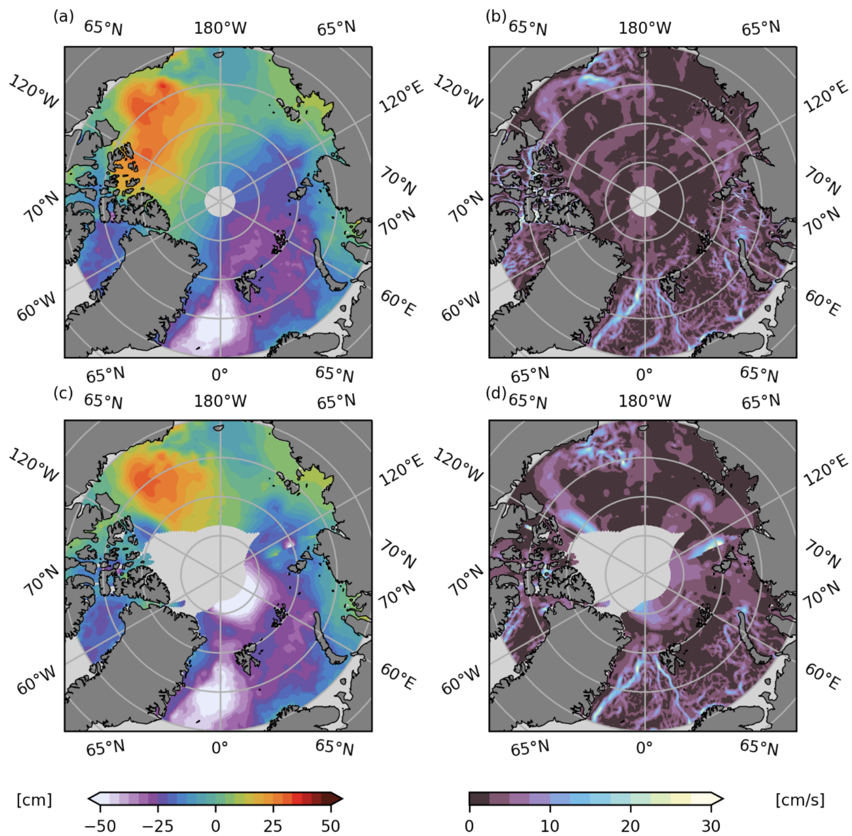

Figure 5: Zoom in on the Artic zone of (a) the CNES-CLS22 MDT (in cm), (b) the amplitude of the associated geostrophic currents (in cm/s), (c) the CNES-CLS18 MDT (in cm) and (d) the amplitude of the geostrophic currents associated with the CNES-CLS18 MDT (in cm/s).

To look at the energy content of MDT, different MDT solutions were compared through a spectral analysis: the first guess (called FirstGuess22), the previous CNES-CLS13 MDT, the previous CNES-CLS18 MDT (Mulet et al. 2021), the DTUUH22 MDT (Knudsen et al. 2022), the new CNES-CLS22 MDT and the Glorys12 numerical model MDT (1/12° numerical model from Mercator-Ocean and distributed within CMEMS: product GLOBAL_REANALYSIS_PHY_001_030,*https://resources.marine.copernicus.eu/?option=com_csw&view=details&product_id=GLOBAL_REANALYSIS_PHY_001_030*).

Figure 6 shows spectral analysis for a 10° box in the Antarctic Circumpolar Current area, between 38°E and 48°E and between 44°S and 54°S. In this zone, the CNES-CLS22 MDT (in black) has significantly more energy than the first guess (noted FirstGuess22, in dashed blue) on scales from 600 km to the smallest, and it is the in-situ data that increase the energy on these scales. The three CNES-CLS MDTs (13 in yellow, 18 in red and 22 in black) follow the energy level and descent of the GLORYS12 model (in green), up to 100km for the CNES-CLS13 MDT, and up to around 60km for the CNES-CLS18 (small offset on the energy level with GLORYS12, but same decrease slope) and the CNES-CLS22 MDT. At the smallest scales, there is still an energy decay towards the smallest scales, but this is less marked than at scales above 60km, probably due to the noise that must be starting to affect these scales. For the CNES-CLS22 MDT, residual scales below 60km, below 30km and below 15km were observed (figures not shown). The MDT fields and associated geostrophic currents show coherent physical structures, but the more we look at the smaller scales the more noise becomes visible; the residual scales below 15km are noisy. Figure 6 also shows the spectrum of the DTUUH22 MDT (in dashed pink), whose energy curve decays more rapidly than GLORYS12 below 300km scales, reaching a plateau around 60-70km, at which scales the noise should start to affect the structures, and then decays more slowly.

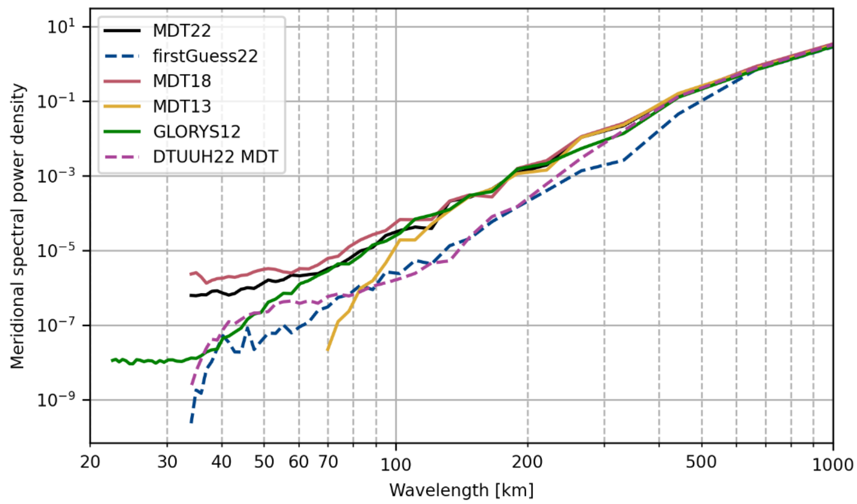

Figure 6: Spectral Power Density obtained for different MDT solutions in a 10°x10° box in the Antarctic Circumpolar Current area for the meridional current, between 38°E and 48°E and between 44°S and 54°S.

4.2 Validation

The validation of the CNES-CLS22 MDT is carried out using different approaches. First, this solution is evaluated qualitatively by region (the European Arctic and the Mid Atlantic Bight), then it is evaluated quantitatively with independent drifter data and then with independent height data estimated from T/S profiles.

4.2.1 Qualitative validation

4.2.1.1 The European Arctic

As seen previously, the CNES-CLS22 MDT provides better coverage of the Arctic region and corrects various CNES-CLS18 artifacts. In this section, we take a closer look at the European Arctic region, and in particular the Yermak Plateau area where the Fram Strait branch of the Atlantic Water flow to the Arctic enters the Polar Basin (fig. 7a), and the St. Anna Trough in the northern Kara Sea which is the main gateway for the Barents Sea branch of the Atlantic Water flow to the Polar Basin (e.g., Schauer et al., 2002, Rudels, 2015; Fig. 7d). We are looking at different solutions for these two areas. For the zoom on the Yermak Plateau, the new CNES-CLS22 MDT solution is shown in Fig. 7a with the bathymetric and geographic elements cited in this section, the CNES-CLS18 MDT solution is shown in Fig. 7b and in 7c the DTUUH2022 solution is shown. For the zoom on the St Anna Through, the CNES-CLS22 MDT solution is shown in Fig. 7d with the geographical elements mentioned, the CNES-CLS18 solution is shown in Fig. 7e and the DTUUH2022 solution in Fig. 7f. A first observation is that the DTUUH2022 solution is smoother than the two CNES-CLS solutions on these two zones.

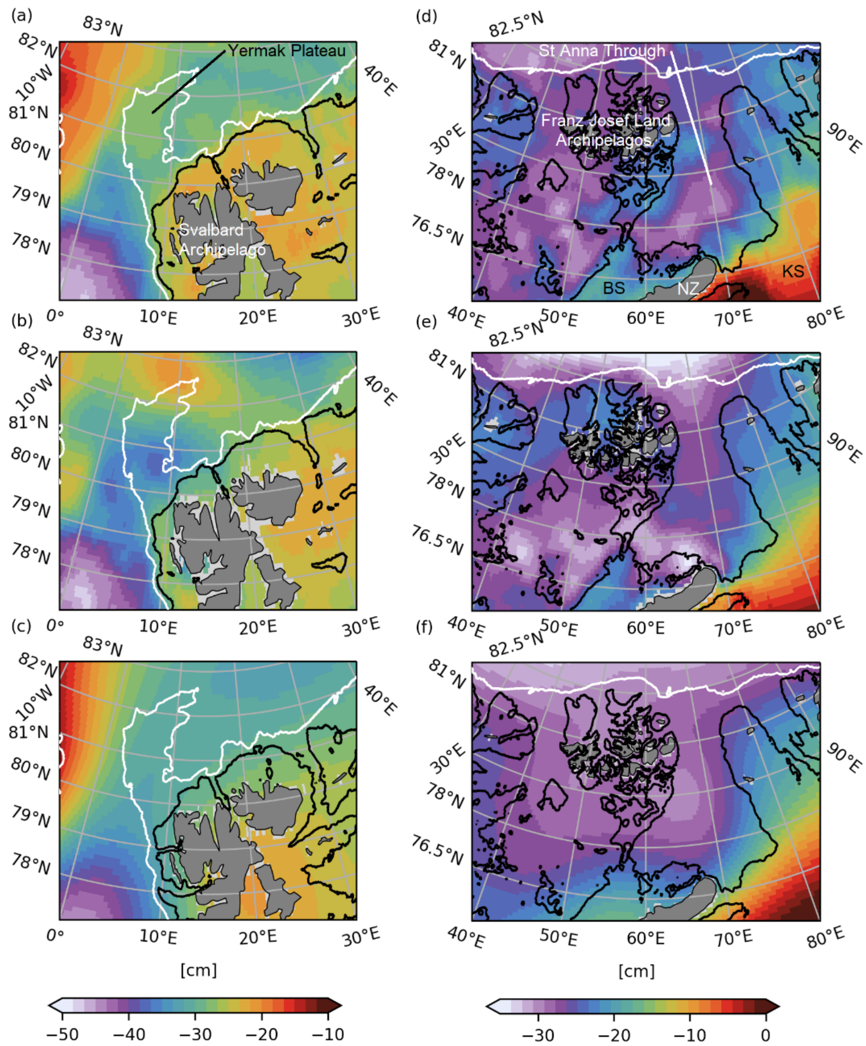

Figure 7: (a) CNES-CLS22 MDT, (b) CNES-CLS18 MDT and (c) DTUUH22 MDT in Yermak Plateau area. The white line represents the 1000m isobath and the black line the 200m isobath. Figure 7a shows the bathymetric and geographical features: the Yermak Plateau and Svalbard Archipelago. (d) CNES-CLS22 MDT, (e) CNES-CLS18 MDT and (f) DTUUH22 MDT in St Anna Through area. The white line represents the 1000m isobath and the black line the 200m isobath. Figure 7d shows the geographical features: the St Anna Through, the Franz Josef Land Archipelago, the Novaya Zemlya (NZ), the Barrents Sea (BS) and the Kara Sea (KS).

In the Yermak Plateau area, where the Fram Strait branch of the Atlantic Water inflow enters the Polar Basin, the CNES-CLS22 MDT shows better alignment of the flow with the bathymetry both for the Svalbard branch crossing the plateau and the Yermak branch going around the plateau (see Fig. 1 in Meyer et al. 2017), compared with the CNES-CLS18 MDT and DTUUH22 MDT.

The CNES-CLS22 MDT also shows some improvements in the St. Anna Trough where the Barents Sea branch of the Atlantic Water flow to the Arctic exits the Barents Sea and enters the Polar Basin. Here, the CNES-CLS22 MDT better aligns with the bathymetry in the northeastern Barents Sea and northern Kara Sea compared with the CNES-CLS18 MDT and DTUUH22 MDT. Moreover, several more detailed differences also better align with features of the flow reported in the literature. The main flow from the Barents Sea is clearly aligned along the bathymetry in the southern part of the trough between the Novaya Zemlya and Franz Josef Land archipelagos (Schauer et al. 2002; Lien and Trofimov 2013), and there is a clear indication of cyclonic circulation of the Fram Strait branch within the same trough (Gammelsrød et al. 2009; Lien and Trofimov 2013). There is also indication of a continuous Novaya Zemlya Coastal Current along the northern tip of Novaya Zemlya (Lien and Trofimov 2013), which is not clearly seen in the CNES-CLS18 MDT and DTUUH22 MDT. Further north in the St. Anna Trough the CNES-CLS22 MDT shows better alignment of the flow with the bathymetry (e.g., Dmitrenko et al. 2015) compared with the smoother DTUUH22 MDT, in addition to more distinct features not seen in the CNES-CLS18 MDT or DTUUH22 MDT. At 81N, there is an indication of a cyclonic eddy previously identified by hydrographic observations, likely caused by the Fram Strait branch entering the St. Anna Trough (Osadchiev et al. 2022). Moreover, a bathymetric feature to the east of the Franz Josef Land archipelago likely affects the southward flowing part of the Fram Strait branch and causes an anti-cyclonic flow as shown in the CNES-CLS22 MDT.

4.2.1.2 Mid Atlantic Bight

As seen in section 2.3, the CNES-CLS22 MDT integrates synthetic geostrophic velocities estimated from high-frequency radar velocities in the Mid Atlantic Bight area on the east coast of the USA between Cape Cod and Cape Hatteras. In this section, the CNES-CLS22 MDT is looked at more precisely in the Mid Atlantic Bight, a region just north of the Gulf Stream with recirculation on the slope and circulation on the continental shelf shown in Fig. 8 (b).

Fig. 8 shows the contours of the CNES-CLS22 MDT (d) in comparison with the CNES-CLS18 MDT (c) and a ROMS model MDT (a). The ROMS model MDT (Fig. 8 (a)) is an average from the ROMS model used in a climatological diagnostic configuration to calculate a kinematically (coastline and bathymetry) and dynamically (ROMS nonlinear model physics) consistent circulation constrained by mean observations of the ocean state and forced by mean surface fluxes and river inflows (details given in Wilkin et al. 2022).

Lentz (2008) and Zhang et al. (2011) have advanced arguments as to the magnitude of the along-shelf sea level gradient in the Mid Atlantic Bight necessary to complete a momentum balance. We expect gentle southwestward flow throughout the Mid Atlantic Bight, and certain recirculation features in the Gulf of Maine and Georges Bank that are clearly evident in the ROMS MDT (Fig. 8 (a)). The across-shelf sea level gradient is consistent with observed southwestward mean currents. Furthermore, the known pattern of geostrophic coastal currents requires that the MDT contours be largely parallel to the coast, which is the case with the ROMS MDT and not always the case with the CNES-CLS18 (Fig. 8 (c)) and 22 (Fig. 8 (d)) MDTs.

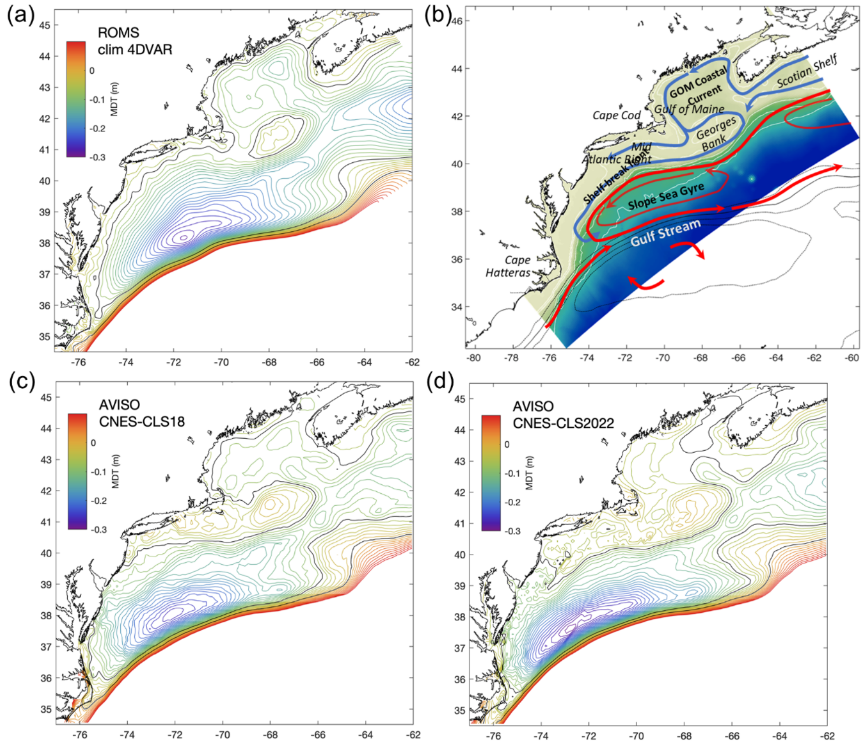

Figure 8: (a) ROMS model MDT contours, (b) Mid Atlantic Bight circulation, (c) CNES-CLS18 MDT contours and (d) CNES-CLS22 MDT contours.

CNES-CLS18 MDT (Fig. 8 (c)) shows a slightly more organized circulation on the shelf, although contours on the inner shelf are noisy. Coastal currents in the Gulf of Maine emerge: Coastal currents on the Scotian Shelf or in the Gulf of Maine are present but weak. In addition, there are still MDT contours cutting the coast, and sea-level slope inversions along the shelf.

The CNES-CLS22 MDT (Fig. 8 (d)) is also noisy on the continental shelf, and there are still contours cutting the coast (associated with low geostrophic velocities). Coastal currents on the Scotian Shelf are more organized, but there still flows into the coast of central New Jersey. So CNES-CLS22 MDT is a significant improvement, but that there is still a way to go to bring MDT to the coast on broad shelves.

4.2.2 Quantitative validation with independent T/S profiles

The CNES-CLS22 and CNES-CLS18 MDTs are compared with independent data. Around 5% of the T/S profiles dataset are randomly selected from 2017 and kept for validation (independent data for CNES-CLS22 and CNES-CLS18 MDTs). The dynamic height estimated from T/S profiles (from a reference depth) characterizes a baroclinic component of the dynamic circulation. Whereas altimetry measures a height that is also influenced by baroclinic processes occurring from the reference depth to the bottom of the water column, and by barotropic processes. For validation purposes, we choose to keep only the deepest profiles (with a reference depth of 1900m), thus reducing the number of deep baroclinic processes not taken into account; this leaves us with a validation set of 2% of the database.

As a first step, we compare the CNES-CLS18 and CNES-CLS22 MDTs against these independent dynamic heights, by looking at the correlation of the ADT (SLA+MDT considered) and the independent dynamic heights (figures not shown). Correlations are calculated in boxes of 5° by 5° (with at least 20 data) and are high, mostly between 0.8 and 1 for both MDTs, and it is difficult to differentiate between them.

Secondly, Figure 9 (a) shows the mean bias per 5°X5° box between the ADT estimated from the CNES-CLS22 MDT and the independent dynamic heights. This global mean bias is 1.30 m, with spatial variations in the Norwegian Sea and to the south near Antarctica (equivalent for CNES-CLS18, not shown) and mainly represents the barotropic component not observed by the dynamic heights. This is why it is removed from the estimate of mean synthetic heights for the calculation of the MDT and the following validation diagnosis on Fig. 9 (b) shows a comparison between the variances of the differences (not considering the bias) between the different ADTs and the dynamic heights, in percent. In blue (in red), the variance of differences is reduced (increased) using CNES-CLS22 compared with CNES-CLS18.

Globally, we see an improvement in CNES-CLS22 MDT compared with CNES-CLS18, but this is not true in all regions. South of the Atlantic and the Indian Ocean (as far south as Australia), the variance of differences is reduced for CNES-CLS22 by more than 10% for many boxes (even if boxes of strong reduction are juxtaposed with boxes of increased variance of differences). Areas of degradation are concentrated in the north-western Atlantic, particularly south of Greenland, in the very north of the Pacific (along the Gulf of Alaska to the Fox Islands, and close to Russia) and in the south of the Pacific, where there are degradations of over 10% (also juxtaposed with improvement boxes).

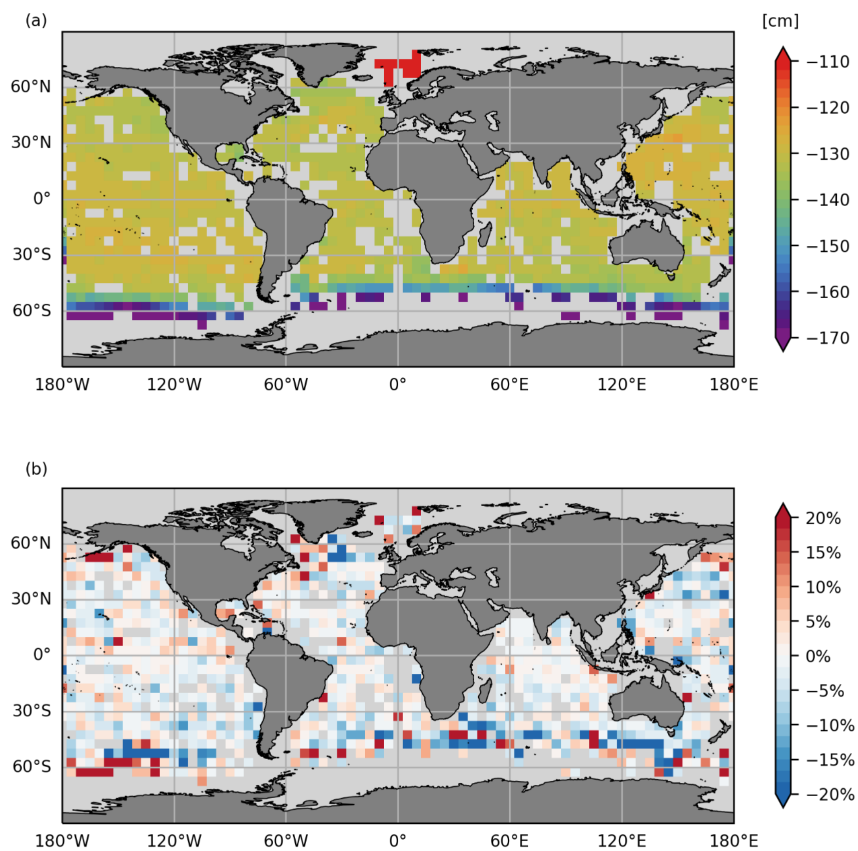

Figure 9: (a) shows the bias in centimetres between the dynamic heights estimated from the independent T/S profiles and the ADT calculated from the CNES-CLS2 MDT. And (b) shows the reduction/increase in variance of the differences between independent dynamic heights and ADT (from CNES-CLS18 and CNES-CLS22) in percent. In blue (in red), the variance of differences is reduced (increased) using CNES-CLS22 compared with CNES-CLS18. All these statistics are calculated in 5°X5° boxes, and only boxes with at least 20 data are kept.

4.2.3 Quantitative validation with independent drifters

The CNES-CLS18 and CNES-CLS22 solutions are compared with independent velocity data. 10% of the AOML drifters dataset are randomly selected and kept for validation (independent data). These drifters are not evenly distributed across the oceans. There are few drifters close to Antarctica (south of about 50°S), at the equator and in Artic. In addition, the Atlantic is slightly better sampled than the other basins, and in particular than the North Indian.

To compare to the MDTs, we remove the wind-driven current (Ekman current and wind slippage for undrogued drifters) from total drifters current and then data are filtered at inertia frequency (if inertia frequency is between 1 and 5 days, otherwise take a minimum of 1 day and a maximum of 5 days) to remove the tide and inertial waves. The objective is to keep only the geostrophic signal. As the geostrophy hypothesis is no longer valid at the equator, we exclude drifters between 5°S and 5°N at the equator.

Absolute dynamic topography values were calculated by adding the CMEMS gridded SLA to the new CNES-CLS22 MDT. Associated geostrophic current were then derived and interpolated along the drifter trajectories. Bias and Root Mean Square differences (RMSD) between the obtained geostrophic velocities with CNES-CLS22 and CNES-CLS18 and the drifter derived geostrophic velocities were calculated spatially by 5°X5° boxes. All these statistics are calculated with at least two different drifters and with at least 100 measurement points.

Comparisons of bias (a) in current modulus (in m/s) and (b) in direction (in degrees) are shown on Figure 10. In blue (in red), there is a decrease (increase) in bias for geostrophic currents derived from the ADT estimated with the CNES-CLS22 MDT. Globally, there is a decrease in bias in current modulus (Figure 10 a) using the new solution, with a greater decrease in bias in areas of strong currents: Gulf Stream, Kuroshio, Agulhas Current and Antarctic Circumpolar Current. The areas of degradation are South Greenland and South Kerguelen. For the directional bias (Figure 10 b), the contribution of the new solution is more mixed, as the direction of geostrophic currents derived from the ADT using the CNES-CLS18 is better in the South between the Kerguelens and southern Australia. These remain areas with fewer validation drifters.

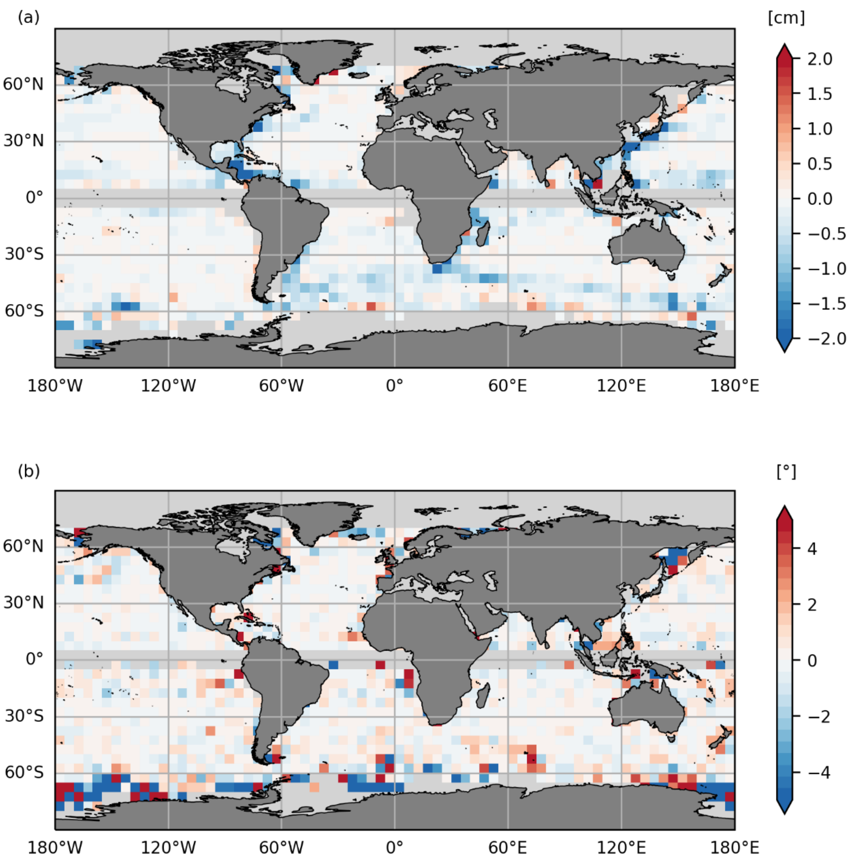

Figure 10: Comparison of bias (a) in current modulus and (b) in current direction independent drifting buoy velocities and the altimeter geostrophic velocities obtained using different MDT solutions. In blue (in red), the bias is reduced (increased) using CNES-CLS22 compared with CNES-CLS18.

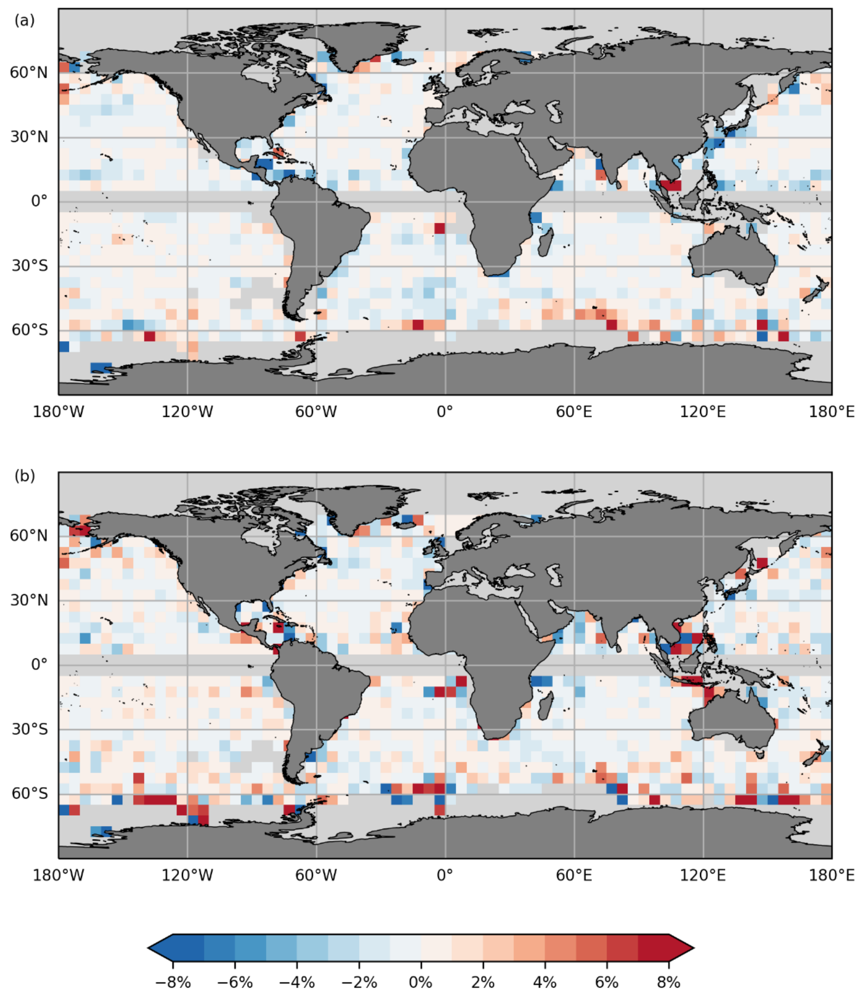

Figure 11: Comparison of the RMS of the differences (a) in current modulus and (b) in direction, of the independent drifting buoy velocities and the altimeter geostrophic velocities obtained using MDT solutions CNES-CLS22 and CNES-CLS18, in percent : $\%\mathrm{RMSD} = \frac{\mathrm{RMS}(\mathbf{U_{ADT22}}) - \mathrm{RMS}(\mathbf{U_{ADT18}} - \mathbf{U_d})}{\mathrm{RMS}(\mathbf{U_{ADT18}} - \mathbf{U_d})}$. In blue (in red), the bias is reduced (increased) using CNES-CLS22 compared with CNES-CLS18. All these statistics are calculated in 5°X5° boxes, and only boxes with at least 2 drifters difters differents and at least 100 measurement points, are kept.

Comparisons of RMS of the differences (a) in current modulus and (b) in direction, of the independent drifting buoy velocities and the altimeter geostrophic velocities obtained using MDT solutions CNES-CLS22 and CNES-CLS18, in percent, are shown are shown on Figure 11. In blue (in red), the RMSD is reduced (increased) using CNES-CLS22 compared with CNES-CLS18. In terms of current amplitude (Figure 11 a), the majority of boxes show an improvement of between 0 and 2.5% for the CNES-CLS22 solution, with in particular a greater improvement at Kuroshio and in the Caribbean Sea. Areas of degradation in current amplitude RMS are the area around Kerguélen in the ACC and along the southeast coast of Greenland. Comparison of the RMS of differences in current direction (Figure 11 b) shows a more mixed result with degradation boxes compared to the CNES-CLS18 solution: in the ACC in the South Pacific. It can also be noted that some boxes show an improvement in the RMS of differences for the CNES-CLS22 solution in current amplitude but not in direction, and vice versa; this is the case for some boxes south of the Kerguélen

Islands and at the extreme south of the Pacific. The areas around the Kerguélen Islands, in the South Pacific between -140°E and -120°E, and around the Fox Islands in the extreme North Pacific remain areas of degradation in RMS of the differences in modulus and current direction for the new solution compared with the previous one. On the other hand, the Kuroshio, the North Atlantic and the Labrador Sea, as well as the Indian Ocean are areas where the RMS of the differences for the new CNES-CLS22 solution has improved compared to the CNES-CLS18 solution.

Globally, the two solutions CNES-CLS22 and CNES-CLS18 remain close with these drifter comparisons, as shown in the following Table 1, which summarizes the drifter comparison statistics over the whole area up to 70°N. Both solutions have a difference RMS of between 10.5 and 11 cm/s for U and V components and current modulus, and a difference RMS of around 34° in direction. The comparison of the two solutions favours the new one, but by less than 1%. It should also be noted that the comparison between the first guess and the CNES-CLS22 MDT shows an improvement in U and V of around 5% in the RMS of differences, and an improvement of around 6% in current amplitude and 2% in direction, which is expected.

RMS(differences)	U [cm/s]	V [cm/s]	M [cm/s]	D [°]
CNES-CLS22 MDT	10,57	10,62	10,79	34,24
CNES-CLS18 MDT	10,59	10,63	10,83	34,26
CNES-CLS22 MDT first guess	11,11	11,17	11,47	35,05
% 22 vs 18	-0,2%	-0,1%	-0,4%	-0,1%
% 22 vs 22 first guess	-4,9%	-4,9%	-5,9%	-2,3%

Table 1: RMS of the differences for the zonal component U, the meridional component V, the current modulus and the direction of the current, of the independent drifting buoy velocities and the altimeter geostrophic velocities obtained using MDT solutions CNES-CLS22, CNES-CLS18 and the CNES-CLS22 first guess. The last two lines show the reduction/increase in RMS of the differences between two solutions: CNES-CLS22 versus CNES-CLS18 and CNES-CLS22 versus CNES-CLS22 first guess, in percent (a negative percentage is a decrease in the RMS of the differences). These statistics were generated using all available drifters up to 70°N.

Given the small number of independent drifters in Arctic, this area is treated separately. Table 2 summarizes the RMS of the differences between the geostrophic currents derived from drifters (degraded treatment) and the geostrophic currents derived from ADTs calculated with the CNES-CLS22, CNES-CLS18 and background CNES-CLS22 solutions. The last two lines show in percent the reduction in RMS of the differences between CNES-CLS22 and CNES-CLS18 MDT and its first guess. In the zonal and meridional components of the current, the new solution reduces the RMS of the differences compared with the drifters by 19% and 12% respectively. This improvement translates into a clear improvement in direction of 9%, which reduces the RMS of the differences from around 56° to 50°; but the RMS of the differences in current amplitude remains very slightly better for CNEs-CLS18. Note that, as the coverage is not quite identical, there are more points taken into account for CNES-CLS22 than for CNES-CLS18.

RMS(differences)	**U [cm/s]**	**V [cm/s]**	**Modulus [cm/s]**	**Direction [°]**
CNES-CLS22 MDT	7,95	8,12	9,61	50,43
CNES-CLS18 MDT	9,86	9,23	9,58	55,88
CNES-CLS22 MDT first guess	7,97	8,26	10,02	51,77
% 22 vs 18	-19,4%	-12,0%	0,4%	-9,8%
% 22 vs 22 first guess	-0,2%	-1,7%	-4,1%	-2,6%

Table 2: RMS of the differences for the zonal component U, the meridional component V, the current modulus and the direction of the current, of the independent drifting buoy velocities and the altimeter geostrophic

velocities obtained using MDT solutions CNES-CLS22, CNES-CLS18 and the CNES-CLS22 first guess. The last two lines show the reduction/increase in RMS of the differences between two solutions: CNES-CLS22 versus CNES-CLS18 and CNES-CLS22 versus CNES-CLS22 first guess, in percent (a negative percentage is a decrease in the RMS of the differences). These statistics are based on the Artic zone north of 80°N. As the CNES-CLS18 MDT has a smaller coverage, the number of points used is slightly different for this solution than for the others.

5 Conclusions

The main improvement of this new CNES-CLS22 MDT over the previous CNES-CLS18 MDT is in the Arctic, with better coverage, no artifacts and a more realistic solution. Globally, the new CNES-CLS22 solution is close to the CNES-CLS18 solution, both have better resolution of small scales than previous CNES-CLS MDTs but are potentially polluted by noise at very short scales. The CNES-CLS22 MDT has been evaluated against independent height and velocity data in comparison with the previous version, the CNES-CLS18. The new solution presents slightly better results, although not identical in all regions of the globe. In particular, the results are better in the Antarctic Circumpolar Current in terms of height, better off Japan and particularly in the Arctic in terms of geostrophic velocities. For geostrophic currents, those of the new CNES-CLS22 MDT in the Antarctic Circumpolar Current are slightly worse than those of the CNES-CLS18 in comparison with drifters.

Improvements to this new MDT include a new first-guess with the CNES-CLS22 MSS and the GOCO06s geoid to which optimal filtering has been applied, as well as Lagrangian filtering at the coast to reduce the intensity of normal currents at the coast, drifting buoy and T/S profile databases have been updated, as have updated processing to obtain synthetic mean geostrophic velocities and synthetic mean heights. In addition, a new type of data, HF radar data, was processed to extract physical content consistent with MDT in the Mid Atlantic Bight region. The study of this region in particular, showed the improvements of CNES-CLS22 MDT, but that there is still work to be done to obtain a more physical solution on the continental shelf. Indeed, on these continental shelves in general, the first guess is not always good because it's close to the coast and today we only process T/S profiles with a depth greater than 200m; we therefore lack data on these shelves. HF radar data can provide some velocities information, as there are few drifting buoy data in these coastal regions, but processing is difficult, as complex and non-negligible ageostrophic currents have to be removed. In the case of the Mid Atlantic Bight, these HF radar data do not allow us to obtain a MDT with a geostrophic flow not crossing the coastline.

Thanks to the new first-guess and in particular the new CNES-CLS22 MSS, the Arctic area is covered in this MDT and the artifacts of CNES-CLS18 have disappeared. Looking more specifically at the European Arctic region, the new CNES-CLS22 solution presents structures in agreement with the literature in the Yermak Plateau area and in the St Anna Through region.

With the arrival of new swath observations from the SWOT (Surface Water and Ocean Topography) satellite launched in December 2022 (Fu et al. 2012), the continuous improvement of MDT accuracy and resolution is necessary. The inclusion of new coastal data, such as HF radar and SAR data, and shallower T/S profiles not currently taken into account, requires a clear separation of geostrophic and ageostrophic processes, and access to physical content consistent with MDT. These treatments call for new methods in order to best process continental shelf areas with varied oceanographic phenomena.

Data availability

The CNES-CLS22 MDT is available on AVISO+ *https://www.aviso.altimetry.fr/en/data/products/auxiliary-products/mdt/mdt-global-cnes-cls.html*

Competing interests

The authors declare that they have no conflict of interest.

Acknowledgements

We thank the beta users for their valuable feedback, and Laurent Berino for his comments on the Artic region.

References

Bingham, Rory J., Keith Haines, and Chris W. Hughes. 2008. "Calculating the Ocean's Mean Dynamic Topography from a Mean Sea Surface and a Geoid." *Journal of Atmospheric and Oceanic Technology* 25 (10): 1808–22.

Bretherton, Francis P., Russ E. Davis, and C. B. Fandry. 1976. "A Technique for Objective Analysis and Design of Oceanographic Experiments Applied to MODE-73." In *Deep Sea Research and Oceanographic Abstracts* , 23:559–82. Elsevier.

Bruinsma, Sean L., Christoph Förste, Oleg Abrikosov, Jean-Michel Lemoine, Jean-Charles Marty, Sandrine Mulet, Marie-Helene Rio, and Sylvain Bonvalot. 2014. "ESA's Satellite-Only Gravity Field Model via the Direct Approach Based on All GOCE Data." *Geophysical Research Letters* 41 (21): 7508–14.

Dmitrenko, Igor A., Bert Rudels, Sergey A. Kirillov, Yevgeny O. Aksenov, Vidar S. Lien, Vladimir V. Ivanov, Ursula Schauer, Igor V. Polyakov, Andrew Coward, and David G. Barber. 2015. "Atlantic Water Flow into the Arctic Ocean through the St. Anna Trough in the Northern Kara Sea: ATLANTIC WATER FLOW TO THE ARCTIC OCEAN." *Journal of Geophysical Research: Oceans* 120 (7): 5158–78. https://doi.org/10.1002/2015JC010804.

Förste, Christoph, Sean.L. Bruinsma, Oleg Abrikosov, Jean-Michel Lemoine, Jean Charles Marty, Frank Flechtner, G. Balmino, F. Barthelmes, and R. Biancale. 2014. "EIGEN-6C4 The Latest Combined Global Gravity Field Model Including GOCE Data up to Degree and Order 2190 of GFZ Potsdam and GRGS Toulouse." GFZ Data Services. https://doi.org/10.5880/ICGEM.2015.1.

Fu, Lee-Lueng, Douglas Alsdorf, Rosemary Morrow, Ernesto Rodriguez, and Nelly Mognard. 2012. "SWOT: The Surface Water and Ocean Topography Mission. Wide-Swath Altimetric Elevation on Earth." https://ntrs.nasa.gov/citations/20120004248.

Gammelsrød, Tor, Øyvind Leikvin, Vidar Lien, W. Paul Budgell, Harald Loeng, and Wieslaw Maslowski. 2009. "Mass and Heat Transports in the NE Barents Sea: Observations and Models." *Journal of Marine Systems*75 (1–2): 56–69.

Hamon, Mathieu, Eric Greiner, Pierre-Yves Le Traon, and Elisabeth Remy. 2019. "Impact of Multiple Altimeter Data and Mean Dynamic Topography in a Global Analysis and Forecasting System." *Journal of Atmospheric and Oceanic Technology* 36 (7): 1255–66. https://doi.org/10.1175/JTECH-D-18-0236.1.

Hersbach, H., B. Bell, P. Berrisford, G. Biavati, A. Horányi, J. Muñoz Sabater, J. Nicolas, et al. 2018. "ERA5 Hourly Data on Single Levels from 1979 to Present. Copernicus Climate Change Service (C3S) Climate Data Store (CDS)." https://doi.org/10.24381/cds.adbb2d47.

Knudsen, P., O. B. Andersen, N. Maximenko, and J. Hafner. 2022. "The DTUUH22MDT Combined Mean Dynamic Topography Model." In . Venise, Italia. https://doi.org/10.24400/527896/a03-2022.3613.

Kvas, Andreas, Jan Martin Brockmann, Sandro Krauss, Till Schubert, Thomas Gruber, Ulrich Meyer, Torsten Mayer-Gürr, Wolf-Dieter Schuh, Adrian Jäggi, and Roland Pail. 2021. "GOCO06s – a Satellite-Only Global Gravity Field Model." *Earth System Science Data* 13 (1): 99–118. https://doi.org/10.5194/essd-13-99-2021.

Lebedev, Konstantin V., Hiroshi Yoshinari, Nikolai A. Maximenko, and Peter W. Hacker. 2007. "Velocity Data Assessed from Trajectories of Argo Floats at Parking Level and at the Sea Surface." *IPRC Technical Note* 4 (2): 1–16.

Lentz, Steven J. 2008. "Observations and a Model of the Mean Circulation over the Middle Atlantic Bight Continental Shelf." *Journal of Physical Oceanography* 38 (6): 1203–21.

Lien, Vidar S., and Alexander G. Trofimov. 2013. "Formation of Barents Sea Branch Water in the North-Eastern Barents Sea." *Polar Research* 32 (1): 18905. https://doi.org/10.3402/polar.v32i0.18905.

Lumpkin, Rick, and Gregory C. Johnson. 2013. "Global Ocean Surface Velocities from Drifters: Mean, Variance, El Niño–Southern Oscillation Response, and Seasonal Cycle." *Journal of Geophysical Research: Oceans* 118 (6): 2992–3006. https://doi.org/10.1002/jgrc.20210.

Meyer, Amelie, Arild Sundfjord, Ilker Fer, Christine Provost, Nicolas Villacieros Robineau, Zoe Koenig, Ingrid H. Onarheim, et al. 2017. "Winter to Summer Oceanographic Observations in the Arctic Ocean North of Svalbard." *Journal of Geophysical Research: Oceans* 122 (8): 6218–37. https://doi.org/10.1002/2016JC012391.

Mulet, Sandrine, Marie-Hélène Rio, Hélène Etienne, Camilia Artana, Mathilde Cancet, Gérald Dibarboure, Hui Feng, et al. 2021. "The New CNES-CLS18 Global Mean Dynamic Topography." *Ocean Science* 17 (3): 789–808. https://doi.org/10.5194/os-17-789-2021.

Osadchiev, Alexander, Kirill Viting, Dmitry Frey, Darya Demeshko, Alina Dzhamalova, Alina Nurlibaeva, Alexandra Gordey, et al. 2022. "Structure and Circulation of Atlantic Water Masses in the St. Anna Trough in the Kara Sea." *Frontiers in Marine Science* 9. https://www.frontiersin.org/articles/10.3389/fmars.2022.915674.

Pail, Roland, Sean Bruinsma, Federica Migliaccio, Christoph Förste, Helmut Goiginger, Wolf-Dieter Schuh, Eduard Höck, Mirko Reguzzoni, Jan Martin Brockmann, and Oleg Abrikosov. 2011. "First GOCE Gravity Field Models Derived by Three Different Approaches." *Journal of Geodesy* 85 (11): 819.

Pegliasco, Cori, Alexis Chaigneau, Rosemary Morrow, and Franck Dumas. 2020. "Detection and Tracking of Mesoscale Eddies in the Mediterranean Sea: A Comparison between the Sea Level Anomaly and the Absolute Dynamic Topography Fields." *Advances in Space Research* , April. https://doi.org/10.1016/j.asr.2020.03.039.

Rio, M. H., S. Guinehut, and G. Larnicol. 2011. "New CNES-CLS09 Global Mean Dynamic Topography Computed from the Combination of GRACE Data, Altimetry, and in Situ Measurements." *Journal of Geophysical Research: Oceans* 116 (C7). https://doi.org/10.1029/2010JC006505.

Rio, Marie Hélène, Ananda Pascual, Pierre-Marie Poulain, Milena Menna, Bàrbara Barceló-Llull, and Joaquín Tintoré. 2014. "Computation of a New Mean Dynamic Topography for the Mediterranean Sea from Model Outputs, Altimeter Measurements and Oceanographic in Situ Data."

Rio, Marie-Helene. 2010. "Absolute Dynamic Topography from Altimetry: Status and Prospects in the Upcoming GOCE Era." *Oceanography from Space* , 165–79.

Rio, M.-H., and F. Hernandez. 2004. "A Mean Dynamic Topography Computed over the World Ocean from Altimetry, in Situ Measurements, and a Geoid Model." *Journal of Geophysical Research: Oceans* 109 (C12). https://doi.org/10.1029/2003JC002226.

Rio, M.-H., S. Mulet, and N. Picot. 2014. "Beyond GOCE for the Ocean Circulation Estimate: Synergetic Use of Altimetry, Gravimetry, and in Situ Data Provides New Insight into Geostrophic and Ekman Currents." *Geophysical Research Letters* 41 (24): 8918–25.

Rio, M.-H., P.-M. Poulain, A. Pascual, E. Mauri, G. Larnicol, and R. Santoleri. 2007. "A Mean Dynamic Topography of the Mediterranean Sea Computed from Altimetric Data, in-Situ Measurements and a General Circulation Model." *Journal of Marine Systems* 65 (1–4): 484–508.

Roarty, Hugh, Scott Glenn, Joseph Brodie, Laura Nazzaro, Michael Smith, Ethan Handel, Josh Kohut, et al. 2020. "Annual and Seasonal Surface Circulation Over the Mid-Atlantic Bight Continental Shelf Derived From a Decade of High Frequency Radar Observations." *Journal of Geophysical Research: Oceans* 125 (11): e2020JC016368. https://doi.org/10.1029/2020JC016368.

Rudels, Bert. 2015. "Arctic Ocean Circulation, Processes and Water Masses: A Description of Observations and Ideas with Focus on the Period Prior to the International Polar Year 2007–2009." *Progress in Oceanography* 132: 22–67.

Schaeffer, Philippe, Marie-Isabelle Pujol, Pierre Veillard, Yannice Faugere, Quentin Dagneaux, Gérald Dibarboure, and Nicolas Picot. 2023. "The CNES CLS 2022 Mean Sea Surface: Short Wavelength Improvements from CryoSat-2 and SARAL/AltiKa High-Sampled Altimeter Data." *Remote Sensing* 15 (11): 2910. https://doi.org/10.3390/rs15112910.

Schauer, Ursula, Harald Loeng, Bert Rudels, Vladimir K. Ozhigin, and Wolfgang Dieck. 2002. "Atlantic Water Flow through the Barents and Kara Seas." *Deep Sea Research Part I: Oceanographic Research Papers*49 (12): 2281–98.

Szekely, Tanguy, Jerome Gourrion, Sylvie Pouliquen, and Gilles Reverdin. 2023. "CORA, Coriolis Ocean Dataset for Reanalysis." SEANOE. https://doi.org/10.17882/46219.

Taburet, Guillaume. 2022. "28 Years of Reprocessed Sea Level Altimetry Products." Presented at the OSTST2022, Venise, Italia. https://doi.org/10.24400/527896/a03-2022.3257.

Wilkin, John, Julia Levin, Andrew Moore, Hernan Arango, Alexander López, and Elias Hunter. 2022. "A Data-Assimilative Model Reanalysis of the US Mid Atlantic Bight and Gulf of Maine: Configuration and Comparison to Observations and Global Ocean Models." *Progress in Oceanography*209: 102919.

Zhang, Weifeng G., Glen G. Gawarkiewicz, Dennis J. McGillicuddy Jr, and John L. Wilkin. 2011. "Climatological Mean Circulation at the New England Shelf Break." *Journal of Physical Oceanography* 41 (10): 1874–93.

Zingerle, P., R. Pail, T. Gruber, and X. Oikonomidou. 2020. "The Combined Global Gravity Field Model XGM2019e." *Journal of Geodesy* 94 (7): 66. https://doi.org/10.1007/s00190-020-01398-0.